Proceedings of the 3rd IASME/WSEAS Int. Conf. on FLUID DYNAMICS & AERODYNAMICS, Corfu, Greece, August 20-22, 2005 (pp195-201)

Numerical Simulation and Hydrodynamic Design Optimization of a Tesla-Type Valve for Micropumps

J. S. ANAGNOSTOPOULOS and D. S. MATHIOULAKIS
School of Mechanical Engineering / Fluids Section
National Technical University of Athens, Greece
Heroon Polytechniou 9, Zografou, 15780 Athens, GREECE
j.anagno@fluid.mech.ntua.gr; mathew@fluid.mech.ntua.gr

Abstract: - A numerical optimization methodology is applied to improve the design of a microchannel structure used in a valveless micropump. The flow simulation algorithm employs the control volume method for Cartesian grids, while advanced numerical techniques are implemented for automatic generation of unstructured, adaptively refined grids and for the representation of irregular boundaries. Several geometric properties of the microchannel are considered as free design variables, and an optimization software based on evolutionary algorithms is used to find the best performance design. The latter is characterized by the ratio of the pressure drop in reverse flow to that in forward flow through the channel, and represents the flow rectification efficiency of the valve, when it is used as a check valve in a reciprocating pump. The optimal design is obtained quite fast and its pressure drop ratio is 50% higher compared to a standard design. Effects of Reynolds number on the valve performance are also examined and presented. Finally, the dynamic behavior of the valve under periodic flow conditions encountered in a reciprocating micropump is simulated and discussed.

Keywords: - Numerical modeling, Hydrodynamic design, Shape optimization, Tesla valve, Valveless micropumps, Unstructured Cartesian grid, Evolutionary algorithms.

1 Introduction

The design and fabrication of microfluidic systems has been an active research field during the last two decades, and numerous microflow devices such as mircochannels, micropumps, flow sensors, filters, mixers, reactors, separators have been drawn, tested, and some of them included in microsystems for medical, biotechnical, environmental and microelectronics cooling applications [1].

A micropump is the most important microfluidic component and its role is to move very small quantities of fluid, of the order of microliters or even nanoliters per minute. Due to its important role in many microfluidic systems, the results of the continuously developing MEMS science on microstructured materials and fabrication technologies are transferred into micropump research, and lots of inventive and innovative devices have been designed and tested [2-4].

The common mechanical micropump is of reciprocating type and consists of a simple cavity closed with a flexible diaphragm that oscillates with the aid of a piezoelectric or electrostatic actuator and causes periodic volume changes of the cavity. During the suction phase the fluid enters the cavity and during the pumping phase the overpressure in the cavity pushes the fluid to the outlet. Such pumps require valves at the inlet and outlet of the chamber to direct the flow into the desired direction. Instead of the conventional check-type valves, valves with no-moving-parts can be alternatively used. The operation principle of the latter is based on the different hydraulic resistance that an especially designed inlet or outlet configuration can induce to the forth and to the back flow direction. In this way, during the suction and the pumping phase the flow enters and exits the chamber through both the inlet and the outlet openings, but the net, average flow is unidirectional. The use of no-moving-part valves increases the pump reliability and usually simplifies the fabrication process. The so-called 'valveless' or 'fixed valves' micropumps are also advantageous when the fluid contains particles or cellular material with size of the order of the flow channels width.

The first reported valveless micropump utilizes a pair of converging/diverging nozzles [5], and since then several valveless micropumps have been realized using this configuration. A 'valvular conduit' structure that was first invented by Tesla [6], offers virtually no resistance to the passage of a fluid in one direction, yet provides significant resistance to fluid flow in the opposite direction. This structure was first studied in a miniature scale for micropump operation by Forster et al. [7], and found to achieve higher flow-rectification efficiency than the diffuser/nozzle element.

The performance of the flow-rectifying element is important for the operation of a valveless micropump, and can be improved using optimum design tools. Numerical optimization is the most promising engineering tool to replace the costly 'build-and-test' method. Three different components are usually combined in this methodology: shape parameterization, computational flow dynamics and cost function minimization. The representation of irregular geometries that are continuously changed during optimization needs a fast and automated grid generation method. Unstructured, body-fitted grids offer a great geometric flexibility and the potential for automation and local refinement [8], but their generation is a formidable task, especially in viscous regions near solid boundaries. The construction of Cartesian grids is the simplest and most straightforward method, but there is a need to simulate grid cells that are cut by the irregular boundaries [9, 10].

In the present work a numerical methodology is applied in order to simulate the flow in a Tesla-type element, as well as to regulate its main design variables for best rectification performance. The recently developed algorithm includes advanced numerical techniques for Cartesian grids and has been successfully applied in various test cases [11, 12]. In order to examine both the steady and the dynamic response of the element for various Reynolds numbers in the laminar region, the simulation is performed in a two-dimensional channel.

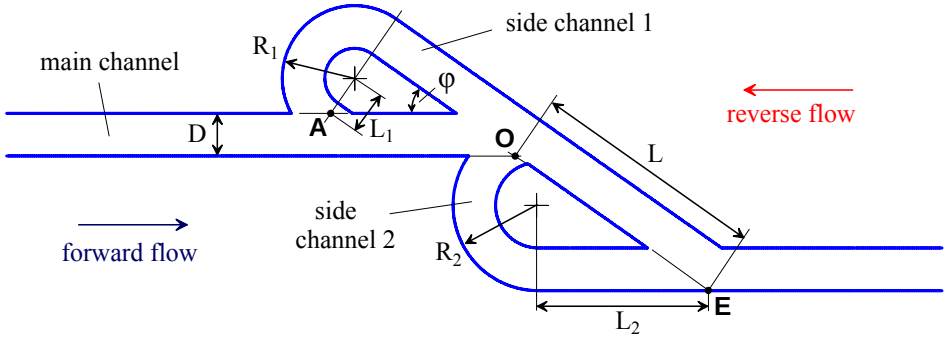

Figure 1. Sketch of the Tesla-type element.

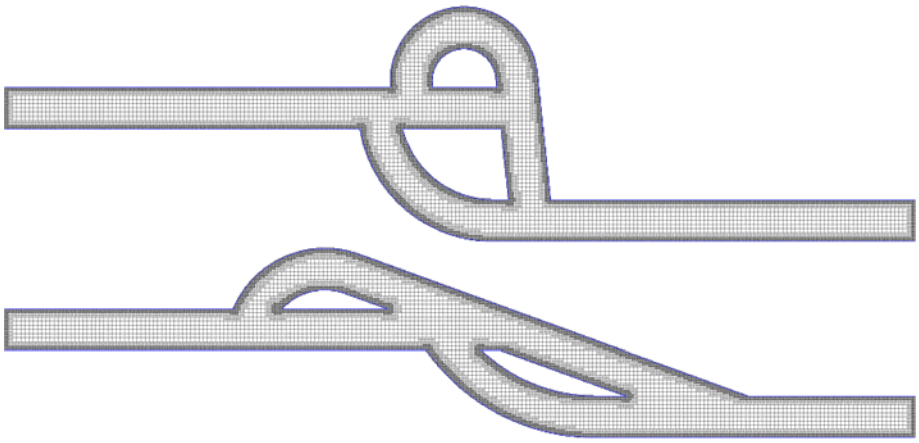

Figure 2. Indicative extreme element shapes.

2 MODEL FORMULATION

2.1 The Tesla-type valve

The microchannel structure shown in Fig. 1 constitutes a single element of Tesla-type design. According to Tesla's concept, the bulk flow in the forward (left-to-right) direction moves along the main central channel, and only a small portion enters the side channels 1 and 2. On the other hand, a significant portion of the flow is forced due to inertia through both side channels when the flow is reversed. Moreover, the flow at the exit of these channels re-enters the main stream at high angles. Consequently, the reverse flow is associated with longer passage lengths, more flow direction changes

and more intense fluid jets confluence, resulting in higher energy losses or pressure drop. Since this element presents higher resistance to the reverse than to the forward flow direction, it can be used in a reciprocating pump as flow rectification valve.

The ratio of pressure drop in the reverse to that in the forward flow direction for a certain flow rate is denoted by the term 'diodicity', D_i, defined as [13]:

$$D_i = \frac{\Delta p_f}{\Delta p_r} \approx \frac{\zeta_f Q^{n_f}}{\zeta_r Q^{n_r}} \quad (1)$$

where the subscripts f and r denote forward and reverse flow, respectively, ζ is a cumulative loss coefficient and Q is the flow rate. In macro-scale pumps the flow is usually turbulent and the viscous losses (n=1) are much lower than the dynamic, inertial losses (n=2). Therefore diodicity is almost equal to the ratio of the two loss coefficients. On the contrary, in microscale channels the Reynolds number is in the laminar region, where the viscous losses become significant. Consequently, diodicity of a Tesla-type valve depends also on the flow rate. Obviously, D_i must be greater than 1 to create a unidirectional net flow.

2.2 Shape parameterization

The design variables used to describe the geometry of the element are shown in Fig. 1. They are the angle φ and the length L of the main channel bend, the radius R_1 and R_2 of the corresponding side channels, and the centers' locations defined by the lengths L_1 and L_2. The maximum possible change in flow direction is 180^o for both side channels. These six variables provide the ability to construct much different shapes, as in the example of Fig. 2. Also, the range of variation of each variable was kept as wide as possible, considering only some geometric constraints (e.g. a fixed total element length, or a minimum main channel length before the first and after the last junction).

2.3 Flow Solver

The finite volume method is used for the solution of the Navier-Stokes equations for the incompressible, viscous flow:

$$\nabla \cdot \vec{V} = 0 \quad (2)$$

$$\frac{\partial \vec{V}}{\partial t} + (\vec{V} \cdot \nabla)\vec{V} = \vec{g} - \frac{1}{\rho}\nabla p + \nu \nabla^2 \vec{V} \quad (3)$$

The equations are discretized according to the collocated arrangement, using a second order upwind scheme, and solved with the Simple algorithm. A preconditioned bi-conjugate gradient (Bi-CG) solver with incomplete ILU decomposition is used. Non-dimensionalized quantities are used in the computations, namely D=1 for the channel width ρ=1 for the fluid density, and u=1 for the mean flow velocity at Re=500.

The unstructured Cartesian grid can be adaptively refined in the vicinity of the channel walls and corners by implementing an advanced flux-conservative methodology that preserves the discretization accuracy [14]. The inclined boundaries do not fit to the Cartesian grid lines and generate 'partially blocked' grid cells that are solved by a numerical technique based on the sharp-interface approach, of almost second order of accuracy [10]. Examples of grid lines arrangement are given in Fig. 2, where adaptive refinement is applied in two successive layers. The maximum cell width for all calculations is 0.05. During the optimization process a new grid is automatically generated for every new set of design variables tested.

2.4 Optimization

The Evolutionary Algorithms SYstem (EASY) optimization algorithm used in this study, is a recently developed and brought to market software at the Lab. of Thermal Turbomachinery, NTUA [15, 16]. The evolutionary optimization methods search for the optimum using populations of candidate solutions instead of a single solution, starting with a randomly selected population. The passage from a population set to the next one, which has more possibilities to contain better solutions, mimics the biological evolution of species generations. EASY utilizes, keeps and evolves three population sets with adjustable population size: parent, offspring and an archival elite set. Binary or real coding can be used along with numerous crossover, mutation and elite operations. Due to its stochastic nature the algorithm can always converge to the global minimum (or maximum) objective value, within a given range of the free design variables. However, the speed of convergence reduces as the number of the design parameters increases.

The flow rectification efficiency of the Tesla-type valve is proportional to its diodicity, therefore the objective of the present design optimization study is to maximize this parameter. In order to obtain the diodicity value for each set of design variables the flow field is solved twice, for a forward and for a reverse constant flow rate, and the pressure differences between the inlet and the outlet cross sections of the element are computed.

3 RESULTS

3.1 Steady-flow response

Some extreme element designs as in Fig. 2 are obviously far from the optimum solution. Indeed, their diodicity values are 1.033 and only 0.903 (reverse net flow), respectively. A more reasonable design is drawn in Fig. 3 according to standard guidelines [13] and will be used as reference case. Its diodicity for Re=500 is computed to 1.6, which is a quite good performance.

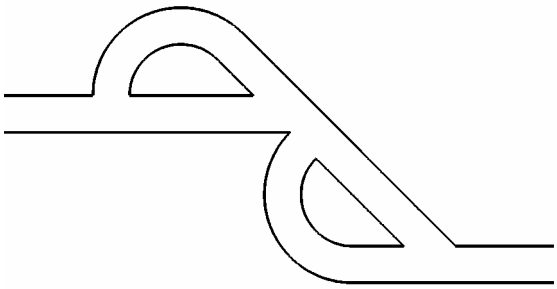

Figure 3. The reference design.

The optimizer is then used to produce the design with the maximum possible diodicity value. The convergence of the algorithm is fast, and as shown in Fig. 4 an optimal solution is practically obtained after about one hundred evaluations. The maximum achievable diodicity is 2.36, namely about 50% higher than that of the reference design.

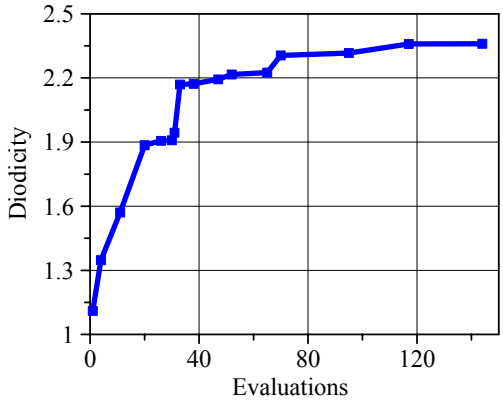

Figure 4. Optimizer convergence history.

The diodicity mechanism can be examined in more detail with the aid of the forward and reverse flow field results for the optimal valve design, drawn respectively in Figs. 5 and 6. The velocity field is much different in forward than in reverse flow. As shown in Figs. 5a and 5b, the bulk forward flow follows the main channel path, and is only slightly disturbed at the side channels junctions. Only 1,3% of the flow bifurcates to the side channel 1 and 4,3% to the side channel 2. The highest velocities remain near the centerline of the main channel even after turning the two corners, exhibiting small separation regions.

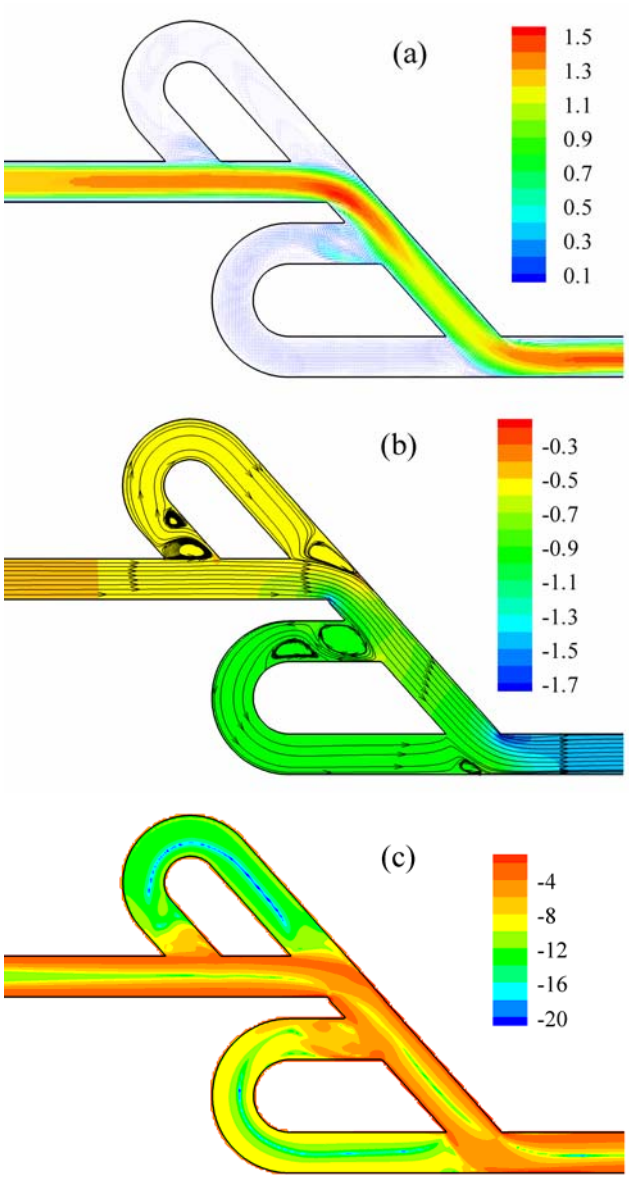

Figure 5. Forward flow field results: a) velocity field; b) streamlines and pressure contours (Pa); c) dissipation energy ($\log_{10}$).

On the other hand, the reverse flow bifurcates at the first junction, and about 55% of it passes through the side channel 2 (Figs. 6a, 6b). The two streams merge again in the sloped section and directed towards the side wall 1, whereas only a 17% of the flow is deflected to the main channel, the majority of which is filled with large recirculation zones. The flow emerges from the side channel 1 as a laminar jet that separates and approaches the opposite wall, thus creating a large and strong recirculation zone in the main channel.

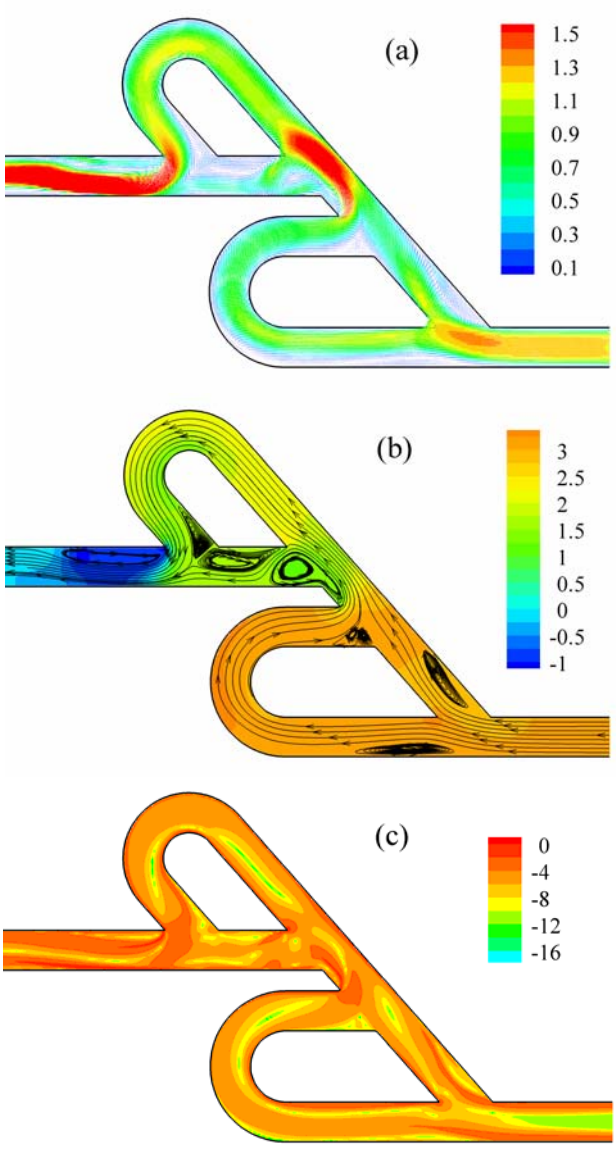

Figure 6. Reverse flow field; legend as in Fig.5.

Significant minor pressure losses in the forward flow are observed only at the two corners of the bend (Fig. 5b), whereas for the reverse flow at the exit of side channel 1 (Fig. 6b). The latter are almost twice as big as the former, and this supports the diodicity of the valve. The rest energy losses in the valve are due to viscous dissipation, in regions of high velocity gradients. The energy dissipation function that involves the viscous stresses is for incompressible, 2D flow [17]:

$$\Phi = \mu\left[2\left(\frac{\partial u}{\partial x}\right)^2 + 2\left(\frac{\partial v}{\partial y}\right)^2 + \left(\frac{\partial u}{\partial y} + \frac{\partial v}{\partial x}\right)^2\right] \quad (4)$$

The base 10 logarithm of the above function is drawn in Figs. 5c and 6c. In the forward flow case no energy dissipation takes place within the side channels where the flow rate is minor. Dissipation occurs along the main channel walls, as well as at the bend corners. The picture is much different in the reverse flow case (Fig. 6c), where the energy dissipation is spread in the whole flow field. In addition to the channel walls, significant velocity gradients exist in both the curved side walls, as well as at the exit junctions where the bifurcated flow streams meet. This behaviour contributes also in the increase of the valve diodicity, mainly in the low Re region.

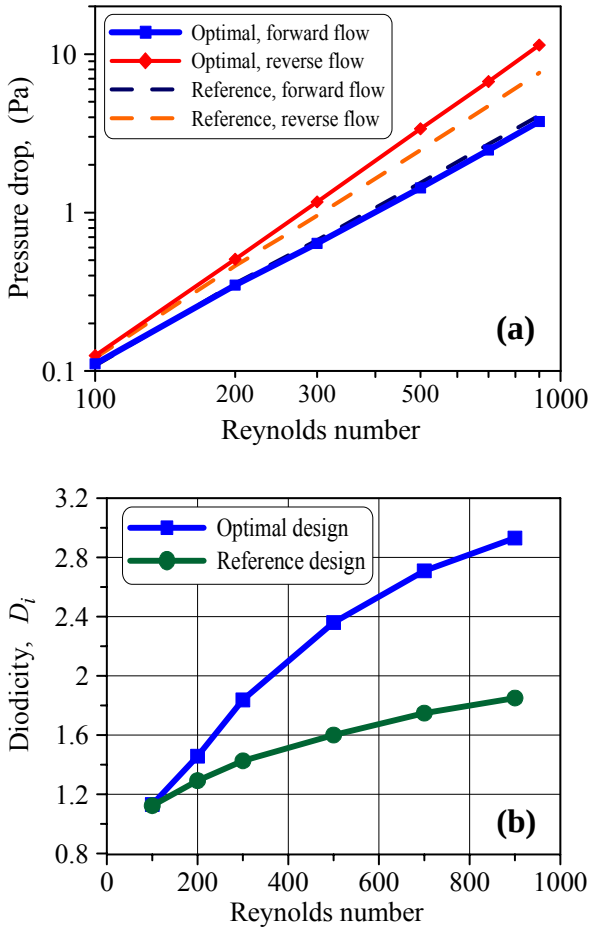

Figure 7. Influence of Re number on the valve pressure drop (a), and Diodicity (b).

The performance of the above optimal design is compared with the reference design (Fig. 3) for various Re in the range 100 to 900 in Fig. 7. The straight lines in the log-log plot of Fig. 7a verify that the flow remains in the laminar region, although there are several flow separation and recirculation regions. The slope of the forward flow data is, as expected, smaller and almost identical for the two designs, whereas the superiority of the optimal design is due to its increased resistance in the reverse flow direction. The diodicity of the optimal design is higher within the whole range (Fig. 7b), and its

relative to the reference design value increases with the Re, up to about 159% for Re=900.

3.2 Transient-flow response

In order to study the transient response of a micropump equipped with Tesla-type valves at the inlet and the exit of its chamber, two such elements of the optimal design are combined and the entire system shown in Fig. 8 is numerically solved. The time variation of the chamber volume and thus of the cumulative flow rate is assumed sinusoidal:

$$Q(t) = V_{max} \cdot 2\pi\, n \cdot sin(2\pi\, n\, t) \qquad (5)$$

where n is the frequency of oscillation, and V_{max} is the stroke volume of the oscillating membrane, the value of which is fixed so as even the maximum possible flow remains in the laminar region.

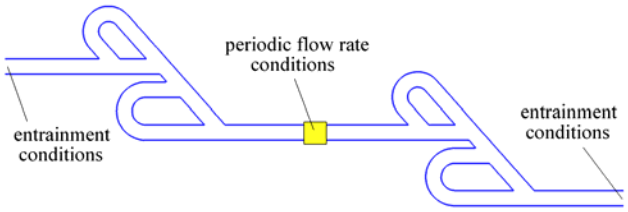

Figure 8. Arrangment for micropump simulation.

The calculations start from a zeroed velocity field, and the oscillating flow rate of the above equation is inserted as source term in the continuity equation of a number of grid cells in the middle of the two Tesla elements (Fig. 8), thus simulating the presence of the pump chamber there. The pressure transient term $\frac{1}{K}\frac{dp}{dt}$ is also added in these equations to account for the elasticity of the oscillating membrane, where the bulk modulus K is fixed to a certain value. The upstream and the downstream edges of the micropump are kept at the same reference pressure (entrainment conditions). In this way, the pressure drop in the left Tesla element is equal to that in the right, but the corresponding flow rates differ due to their different resistance.

The results for the pump flow rate at various driving frequencies are plotted in Fig. 9. In order to reach to a final, periodic field, a number of successive complete cycles need to be simulated, which varies from some tens up to several hundreds, depending on the frequency value. At low frequencies the model exhibits a quasistatic behavior and the net flow rate increases with the frequency, while maximum rates are obtained for the resonance frequency at about 22.5 Hz. In that case the net pump flow rate becomes 35% of its volume stroke rate. At higher frequencies both the forward and the reverse flow rates decrease due to the phase shift between actuation and membrane displacement, and the same is valid for the net pump rate in Fig. 9. This behavior is in agreement with analogous measurements and simulations in the literature [3,4].

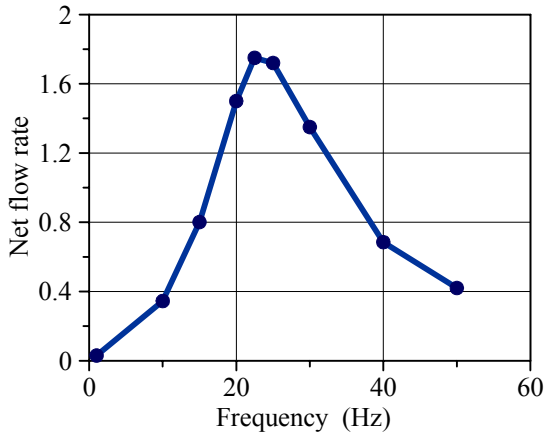

Figure 9. Dynamic response of the micropump.

4 Conclusions

Numerical simulation of a Tesla-type microchannel element is carried out to examine the details of the diodicity mechanism, as well as to optimize its geometry for best flow rectification performance. In the laminar flow region, which is usually encountered in microfluidic systems, both dynamic and viscous effects contribute to the flow energy losses and determine the diodicity of the examined valve. The obtained optimal design exhibits about 50% higher diodicity than the standard one, showing that the used methodology is an efficient tool in hydrodynamic design. Moreover, the developed model is capable to reproduce the transient behavior of the entire micropump device, at different driving frequencies.

References:

[1] S. Shoji and M. Esashi, Microflow devices and systems, *J. Micromech. Microeng.*, Vol.4, 1994, pp. 157-171.

[2] N.T. Nguyen, X. Huang, and T.K. Chuan, MEMS-Micropumps: A Review', *Trans. ASME, J. Fluids Engin.*, Vol.124, 2002, pp.384-392.

[3] D.J. Laser and J.G. Santiago, A review of micropumps, *J. Micromech. Microeng.*, Vol.14, 2004, pp.R35–R64.

[4] P. Woias, Micropumps–past, progress and future prospects, *Sensors & Actuators B*, Vol.105, No.1, 2005, pp. 28-38.

[5] E. Stemme and G. Stemme, A valveless

diffuser/nozzle-based fluid pump, *Sensors & Actuators* A, 1993, Vol.39, pp. 159-167.

[6] N. Tesla, Valvular conduit, *U.S. Patent No. 1.329.559*, 1920.

[7] F.K. Forster, R.L. Bardell, A.P. Blanchard, M.A. Afromowitz, and N.R. Sharma, Micropumps with fixed valves, *U.S. Patent 5.876.187*, 1999.

[8] B.K. Soni, Grid generation: Past, present and future, *Appl. Num. Mathematics*, Vol.32, 2000, pp. 361-369.

[9] H.S. Udaykumar, R. Mittal, P. Rampunggoon, and A. Khanna, A sharp interface Cartesian grid method for simulating flows with complex moving boundaries, *J. of Comp. Physics*, Vol.174, 2001, pp. 345-380.

[10] J.S. Anagnostopoulos and G. Bergeles, 3-Dimensional modeling of the flow and the interface surface in a continuous casting mold model, *Metall. & Mater. Trans. B*, Vol.30, 1999, pp. 1095-1105.

[11] V.A. Grapsas and J.S. Anagnostopoulos, Numerical optimization of the hydrodynamic shape of fluid flow systems', *1st Intl Conference, From Scientific Computing to Computational Engineering, IC-SCCE*, Athens, 8-10 September 2004.

[12] V.A. Grapsas, J.S. Anagnostopoulos, and D.E. Papantonis, Hydrodynamic design of a radial flow pump impeller by surface parameterization, *1st Intl. Conference on Experiments/Process/System Modelling/Simulation/Optimization*, Athens, 6-9 July, 2005.

[13] F.K. Forster, R.L. Bardell, M.A. Afromowitz, N.R. Sharma, and A. Blanchard, Design, Fabrication and Testing of Fixed-valve Mocro-pumps, *Proc. ASME Fluids Eng. Div., IMECE* 1995, Vol.234, 1995, pp. 39-44.

[14] J.S. Anagnostopoulos, Discretization of transport equations on 2D Cartesian unstructured grids using data from remote cells for the convection terms, *Intl. J. for Num. Meth. in Fluids*, Vol.42, 2003, pp. 297-321.

[15] K.C. Giannakoglou, Design of optimal aerodynamic shapes using stochastic optimization methods and computational intelligence, *Progr. in Aerospace. Sci.*, Vol.38, 2002, pp. 43-76.

[16] M.K. Karakasis, A.P. Giotis, and K.C. Giannakoglou, Inexact information aided, low-cost, distributed Genetic Algorithms for aerodynamic shape optimization, *Intl. J. Num. Methods Fluids*, Vol.43, 2003, pp. 1149-1166.

[17] F.M. White, *Viscous Fluid Flow*, 2nd ed., McGraw-Hill, 1991.